Atmos. Chem. Phys. Discuss., doi:10.5194/acp-2016-874, 2016
Manuscript under review for journal Atmos. Chem. Phys.
Published: 8 November 2016

Atmospheric Chemistry and Physics Discussions

Day- and Night-time Formation of Organic Nitrates at a Forested Mountain-site in South West Germany

Nicolas Sobanski[1], Jim Thieser[1], Jan Schuladen[1], Carina Sauvage[1], Wei Song[1], Jonathan Williams[1], Jos Lelieveld[1] and John N. Crowley[1]

[1] Max-Planck-Institut für Chemie, Division of Atmospheric Chemistry, Mainz, Germany.

Correspondence to: J. N. Crowley (john.crowley@mpic.de)

Abstract. We report in-situ measurement of total peroxy-nitrates (ΣPNs) and total alkyl nitrates (ΣANs) in a forested / urban location at the top of the Kleiner Feldberg mountain in South-West Germany. The data, obtained using Thermal Dissociation Cavity Ring Down Spectroscopy (TD-CRDS) in August-September 2011 (PARADE campaign) and July-August 2015 (NOTOMO campaign), represent the first detailed study of ΣPNs and ΣANs over continental Europe. We find that a significant fraction of NO*x* (up to 75 %) is sequestered as organics nitrates at this site. Futher, we also show that the night-time production of alkyl nitrates by reaction of NO_3 with biogenic hydrocarbons is comparable to that from day-time, OH-initiated oxidation pathways. The ΣANs-to-ozone ratio obtained during PARADE was used to derive an approximate, average yield of organic nitrates at noon time from the OH initiated oxidation of VOCs of 7 % at this site in 2011, which is comparable with that obtained from an analysis of VOCs at the site. A much lower yield, < 2 %, was observed in 2015, which may reflect a reduction in the fraction of biogenic hydrocarbons contributing to OH reactivity in that year.

1 Introduction

The gas- and aerosol-phase chemistry of the continental, tropospheric boundary layer is strongly influenced by reactive nitrogen oxides. The primary pollutants NO and NO_2 (constituting the NO*x* family) are mostly emitted by anthropogenic activity involving high temperature combustion or from microbial activity in soils and have a strong impact on tropospheric O_3 levels. Knowing the fate of NO*x* is paramount to prediction of O_3 production rates and oxidation capacity on regional and global scales (Lelieveld et al., 2016). Following emission, NO undergoes a series of reaction steps that ultimately lead either to the formation of short lived trace gases that can act as sinks for NO*x* (HNO_3) or to the formation of longer lived, reservoir species that can be transported over long disances and act as a source of NO*x* ($RONO_2$ and $RC(O)OONO_2$) in locations that are remote from anthropogenic emissions. In the troposphere, a significant amount of NO*x* can be temporarily sequestered as HNO_3 and organic nitrates. The former is produced predominantly by the oxidation of NO_2 by OH whereas organic nitrates are produced by the oxidation of both NO and NO_2 by organic peroxy radicals during the day (R3 and R4) or in the oxidation

Atmos. Chem. Phys. Discuss., doi:10.5194/acp-2016-874, 2016
Manuscript under review for journal Atmos. Chem. Phys.
Published: 8 November 2016

Atmospheric Chemistry and Physics Discussions

of alkenes by NO_3 during the night (R6) (see below). Organic peroxy radicals are formed in the oxidation of hydrocarbons by OH (R1 and R2) (Atkinson, 2000; Atkinson and Arey, 2003a, b).

The products of NO*x* oxidation by organic radicals are peroxy nitrates (RO_2NO_2, abbreviated as PNs, R3) and alkyl nitrates ($RONO_2$ abbreviated called ANs, R4). Based on thermal lifetimes, PNs may be divided divided in two families, those with a carbonyl group adjacent to the peroxy entity (i.e. $RC(O)O_2NO_2$) and those without. The former are peroxyacyl nitric anhydrides, generally referered to as peroxyacyl nitrates or PANs, and have lifetimes with respect to thermal dissociation on the order of hours in the midlatitude boundary layer. Non-acyl PNs (RO_2NO_2) such as $CH_3O_2NO_2$ and HO_2NO_2 thermally decompose on timescales of seconds to minutes at temperatures close to 298 K and are thus only encountered in significant concentrations in cold regions of the atmosphere (Murphy et al., 2004; Browne et al., 2011; Nault et al., 2015). Alkyl nitrates are formed with variable branching ratio in a minor channel (R4) of the reaction between organic peroxy radicals and NO, the greater fraction of this reaction leading to formation of an alkoxy radical and NO_2 (R5) and thus (via NO_2 photolysis) ultimately to O_3. Alkyl nitrates are also formed at night during the NO_3 induced oxidation of unsaturated hydrocarbons, the first reaction step being addition of NO_3 to a double bond followed by formation of a nitrooxy alkylperoxy radical (R6), the fate of which includes reaction with HO_2, other peroxy radicals, NO_3, NO_2 or, if available, NO so that the final products are, hydroxy-, hydroxide- and carbonyl- substituted nitrates as well as dinitrates (Schwantes et al., 2015; IUPAC, 2016). The nitrate yields (per VOC reacted) can be high, especially for biogenic VOCs including the terpenoids, and can exceed 50 % (Ng et al., 2016).

Organic nitrates have highly variable lifetimes (from seconds to days) that are mainly controlled by rates of thermal decomposition and thus temperature for PNs. For ANs, OH oxidation, photolysis and deposition or scavenging by aerosol particles all play a role (Roberts, 1990; Browne et al., 2013; Rollins et al., 2013).

$OH + RH (+ O_2)$	$\rightarrow$	$RO_2 + H_2O$	(R1)
$R{=}R' + OH (+ O_2)$	$\rightarrow$	$R(OH)R'O_2$	(R2)
$RO_2 + NO_2 + M$	$\rightarrow$	$RO_2NO_2 + M$	(R3)
$RO_2 + NO + M$	$\rightarrow$	$RONO_2 + M$	(R4)
$RO_2 + NO$	$\rightarrow$	$RO + NO_2$	(R5)
$R{=}R' + NO_3 (+ O_2)$	$\rightarrow$	$R(ONO_2)R'O_2$	(R6)
$R(ONO_2)R'O_2$ (+ROx, NOx)	$\rightarrow$	ANs	(R7)

The first field measurements of organic nitrates were made using low time resolution methods (gas chromatography) (Roberts et al., 1989; Blanchard et al., 1993) and focused mostly on PAN (peroxy acetyl nitrate), PPN (peroxy propyl nitrate) and MPAN (methacryloyl peroxynitrate) (Williams et al., 1997; Williams et al., 2000) which are the most common peroxy nitrates in the continental boundary layer, and individual mono- and polyfunctional alkyl nitrates from alkane or alkene

Atmos. Chem. Phys. Discuss., doi:10.5194/acp-2016-874, 2016
Manuscript under review for journal Atmos. Chem. Phys.
Published: 8 November 2016

precursors (Atlas, 1988; Flocke et al., 1991). More recently, mass spectrometry based methods have been developed to measure a wider range of organic nitrates at high time resolution (Beaver et al., 2012). Early attempts to compare speciated NO_y and total NO_y measurements (Fahey et al., 1986; Buhr et al., 1990; Ridley et al., 1990) revealed a substantial missing fraction of reactive nitrogen which was addresssed by the first measurements of ΣPNs and ΣANs by thermal dissociation coupled with laser induced fluorescence detection of NO_2 (Day et al., 2003). Those and subsequent measurements (Wooldridge et al., 2010; Perring et al., 2013) indicated that, depending on environment, the interaction between NO*x* and VOCs leads to a wide variety of compounds with different level of structural functionality and atmospheric lifetime which can have a variable and significant influence on the lifetime of NO*x* and also aerosol particles composition (Browne et al., 2013; Ayres et al., 2015).

We present here an analysis of organic nitrates and NO_2 measured using TD-CRDS during two field campaigns that took place at a forested, semi-rural mountain site in South-Western Germany. As far as we are aware, this work constitutes the first measurement and analysis of ΣPNs and ΣANs over continental Europe. We show that the daily variations of ΣANs and ΣPNs are both controlled by photo-chemical oxidation of VOCs, night-time production by NO_3 induced oxidation of biogenic VOCs and local meteorology. We also report an estimation of the effective branching ratios of AN formation in R4 and R5 using O_3 measurements and compare this with an estimation based on VOCs at the site and known, individual branching ratios.

2 Campaign site and meteorology

The PARADE (PArticles and RAdicals: Diel observations of the impact of urban and biogenic Emissions) and NOTOMO (NOcturnal chemistry at the Taunus Observatory: insights into Mechanisms of Oxidation) campaigns took place during August-September 2011 and July-August 2015 at the Taunus Observatory (50.22 N, 8.45 E) on top of the "Kleiner Feldberg" mountain, 850 m above sea-level and 500 m above nearby urban centres in the states of Hessen and Rheinland-Pfalz in South-Western Germany. This site has been described extensively in different publications (Crowley et al., 2010; Sobanski et al., 2016b) and only a short description is given here. A few km to the NNE and SE of the station are two mountains of similar height ("Großer Feldberg" 878 m and "Altkoenig" 798 m ASL). The nearby (10s of km) environment in the complete northern sector is a partially forested, rural region. The SW-SE sector is a more densely populated, industrialized region which includes the Frankfurt-Mainz-Wiesbaden urban agglomeration. Frankfurt is situated ≈ 20 km to the SE and Mainz and Wiesbaden ≈ 20 – 30 km to the SW. A detailed land-use analysis of the surrounding area was given by Sobanski et al. (2016b).

Reactive trace-gas measurements at the site are strongly influenced by the horizontal advection of different types of air masses, both on a local scale (forest/rural vs. urban) and on regional scales (continental vs. marine). On some nights during PARADE, the instruments sampled air from a low lying residual layer which resulted in very high NO_3 steady state lifetimes (≈ 1h) (Sobanski et al., 2016b). During both campaigns, the meteorological conditions were very variable and associated

Atmos. Chem. Phys. Discuss., doi:10.5194/acp-2016-874, 2016
Manuscript under review for journal Atmos. Chem. Phys.
Published: 8 November 2016

with different air mass origins. The PARADE campaign can be divided in three periods (Phillips et al., 2012). The first period from the 15th to the 26th of August was influenced by air masses of continental origin and was associated with high temperature, and low humidity. A cold front arriving from the West resulted in two consecutive days of rain/fog conditions and a large decrease in temperature and ozone. The period 26th to 5th of September was influenced by advection from the Atlantic / UK region and during this period the temperature increased progressively together with ozone. A second cold front on the 5th of September again resulted in a fast temperature decrease followed by a period of low photochemical activity. The NOTOMO campaign was characterised by frequent fluctuation between cold/wet and warm/dry periods. Back trajectory calculations (48 hrs) showed that the warm/dry periods were generally associated with air masses of continental origin, the cold/wet periods with air masses coming from the West with Atlantic influence. In both campaigns, the highly variable photochemical activity and temperature strongly influenced the mixing ratios of both O_3 and organic nitrates, which is why this site was selected.

3 Instrumentation

The instruments deployed during both field campaigns have been described in Schuster et al. (2009) and Thieser et al. (2016) for PARADE and in Sobanski et al. (2016a) for NOTOMO. During the PARADE campaign, all instruments used collocated inlets of PFA piping. During the NOTOMO campaign, the instruments described here sampled from a common, high volume-flow inlet. Temperature, ozone, wind speed and wind direction data were measured by the permanent instrumentation of the state-run air pollution surveillance network (HLUG) at this site.

3.1 NO_2, NO_3, ΣPNs and ΣANs

PARADE: NO_2 and total organic nitrates were measured during both campaigns by Thermal Dissociation Cavity Ring-Down Spectroscopy (TD-CRDS). During PARADE, a two cavity TD-CRDS instrument was deployed (Thieser et al., 2016). The instrument was located in a container and sampled air from a 5 m ½" PFA tube acting as a bypass flow through which ambient air was drawn at ≈ 40 dm^3 (STP) min^{-1}, (hereafter SLM). The Teflon coated (DuPont, FEP, TE 9568) cavities were operated at 405 and 409 nm, and both were maintained at 35 °C to improve thermal stability. One cavity sampled air from the bypass flow at ambient temperature to measure NO_2 mixing ratios, the second channel sampled alternately through two heated inlets, one held at 200 °C and the other at 450 °C to thermally dissociate PNs and ANs respectively into NO_2. When sampling through the 200 ° C inlet, this channel measures the sum of ambient NO_2 + ΣPNs. Sampling via the 450 °C inlet results in detection of NO_2 + ΣPNs + ANs. Mixing ratios of ΣPNs and ΣANs were obtained by the difference in NO_2 measured in the two cavities and applying corrections to account for conversion (to NO_2) of $ClNO_2$ (measured by CIMS, Phillips et al. (2012)) and N_2O_5 (TD-CRDS, Sobanski et al. (2016b)) in the hot inlets and also for biases related to reactions involving peroxy radicals, NO, NO_2, and O_3 as outlined in detail in Thieser et al. (2016).

During PARADE, NO_3 was measured by the 662 nm, two channel TD-CRDS described in Schuster et al. (2009). One cavity sampled air at ambient temperature and measured NO_3, the second one measured the sum of NO_3 and N_2O_5 following the

Atmos. Chem. Phys. Discuss., doi:10.5194/acp-2016-874, 2016
Manuscript under review for journal Atmos. Chem. Phys.
Published: 8 November 2016

Atmospheric Chemistry and Physics Discussions

thermal dissociation of N_2O_5 to NO_3 and NO_2 at 100 °C. This instrument was located on the roof top and sampled air from the centre of a bypass flow (50 SLM) through a 1 m long, ½-inch (12.7 mm) diameter PFA pipe. The detection limit for NO_3 and NO_2 were 2 and 30 pptv and the uncertainties 15 and 6 % respectively. As described in Thieser et al. (2016), the uncertainty associated with the NO_2 measurement is 6 % + 20pptv × RH/100 (where RH is the relative humidity in %). The detection limit and uncertainties for the organic nitrate meaurements depends on NO*x* levels and the reader is referred to Thieser et al. (2016) for more details.

NOTOMO: The 5 channel, TD-CRDS deployed during the NOTOMO campaign was recently decribed in detail by Sobanski et al. (2016a). This instrument has five identical cavities sampling from separate inlet lines. Two cavities operate at 662 nm for the detection of NO_3, the other three at 405 nm to detect NO_2. One 662 nm cavity samples 8 SLM from an inlet at ambient temperature to measure NO_3, the other draws 7 SLM through an inlet at 110 °C to measure the sum of NO_3 + N_2O_5 following thermal dissociation of N_2O_5 to NO_3. Of the three 405 nm cavities, one draws 2.5 SLM via an inlet at ambient temperature to measure NO_2, the other two each sample 2.5 SLM from inlets heated to 175 °C and 375 °C to measure NO_2 + ΣPNs and NO_2 + ΣPNs + ΣANs, respectively. The ¼ inch (6.35 mm) inlet line for the 662 nm cavities was attached ia a T-piece to a 60 cm long ½ inch PFA pipe sampling air at 100 L min^{-1} from the center of a large diameter (15 cm), high-flow inlet (10 m^3 min^{-1}), with its opening located 8 m above the ground and 3m above the top of the container. The 405 nm channels sampled air via a 1 m long, ¼ inch PFA tube protruding into the center of the high-flow inlet. Correction for $ClNO_2$ and N_2O_5 conversion to NO_2 were carried out as described for the PARADE campaign, the removal of the biases related to reactions by peroxy radicals, O_3 and NO*x* were carried out as described in Sobanski et al. (2016a). The detection limits were 1.5 and and 60 pptv for NO_3 and NO_2, respectively, with uncertainties of 25 % for NO_3 and 6.5 % for NO_2 (Sobanski et al., 2016a).

3.2 NO during PARADE / NOTOMO

During PARADE, NO measurements were made with a modified commercial chemiluminescence detector (CLD 790 SR), the operation of which during this campaign is described by Li et al. (2015). The detection limit for this instrument is 4 pptv in 2 s with a total uncertainty of 4 %. This instrument did not participate in NOTOMO and daytime NO mixing ratios were calculated from measurements of NO_2, O_3 and $J(NO_2)$ assuming photo stationary state:

$$[NO]_{calc} = J(NO_2)\,[NO_2] / k_{(NO+O3)}[O_3] \quad (1)$$

where $J(NO_2)$ is the photolysis frequency of NO_2 and $k_{(NO+O3)}$ is the rate constant for reaction of NO with O_3. This expression ignores the oxidation of NO to NO_2 via e.g. reactions of peroxy radicals and thus overestimates NO. However, this method of estimating [NO] resulted in satisfactory agreement (within ≈ 20 %) with measurements from the HLUG for periods when NO was above the detection limit (> 1ppb) of their instrument. Night-time concentrations of NO during NOTOMO were

Atmos. Chem. Phys. Discuss., doi:10.5194/acp-2016-874, 2016
Manuscript under review for journal Atmos. Chem. Phys.
Published: 8 November 2016

assumed to be zero, as has been shown to be the case on many nights during previous campaigns at this site (Crowley et al., 2010; Sobanski et al., 2016b).

3.3 VOCs measurements during PARADE

The VOC measurements have been described already by Sobanski et al. (2016b). Briefly, VOCs were measured using two gas-chromatographic instruments (1 data point per hour) with a mass spectrometer (GC-MS) and a flame ionisation detector (GC-FID). The GC-MS (biogenic and aromatic hydrocarbons) had a detection limit of around 1 pptv with an uncertainty of 10–15 %. The GC-FID (non-methane hydrocarbons) had detection limits between 1 and 5 pptv, exceptions being ethane, ethene, propene, benzene and toluene with values of 8, 16, 9, 14 and 48 pptv respectively and a total uncertainty of 10 % (15 % for 1-pentane). The VOCs measured during PARADE are listed in Table 1 along with their rate constants for reaction with OH and also the associated alkyl nitrate yields and production rates, P(ANs) and P(O_3), for ANs and PNs, respectively (see Sect. 4.4).

4 Results and discussion

4. 1 NO*x* and organic nitrates at the Taunus Observatory

The temperature, humidity, wind direction, O_3, NO, NO_2, ΣPNs and ΣANs for the PARADE and NOTOMO campaigns are shown in Fig. 1 and Fig. 2., respectively. The reactive nitrogen species are plotted at 10 min resolution, and Table 2 summarizses selected minimum, maximum and mean values for the two datasets. The data provided by the HLUG (relative humidity, wind and O_3) are given at 30 min intervals.

During PARADE and NOTOMO, NO_2 varied between ≈ 1 to 15 ppbv with the highest mixing ratios (during PARADE) associated with air mass originating from the south and from the south - west, corresponding approximately to the urbanized Frankfurt and Wiesbaden/Mainz sectors. The ΣPNs mixing ratio varied from below the detection limit to ≈ 3 ppbv during NOTOMO. Low values approaching or below the detection limit were measured during episodes of persistent fog and rainfall. The campaign means for ΣPNs were 505 pptv for PARADE and 677 pptv for NOTOMO, respectively. ΣANs mixing ratios varied from below the detection limit to 1.2 ppbv (PARADE maximum) with campaign mean values of 297 pptv for PARADE and 116 pptv for NOTOMO, repectively. Figures 1 and 2 show that [ΣPNs] and [ΣANs] covary at the Taunus Observatory and also show a correlation with O_3 both in terms of their diel profile (see later) and day-to-day variability.

Measurements of individual peroxyacyl nitrates are numerous, especially of PAN which usually represents ~ 80% of all peroxy-nitrates in the lower troposphere (Roberts, 1990; Roberts et al., 1998). This has been shown to also be the case at the Taunus Observatory (Thieser et al. 2016). Our measurements of [ΣPNs] are in the range of [PAN] or the sum of individual PANs mixing ratios observed in different urban/suburban locations (Roberts, 1990; Roberts et al., 2007; LaFranchi et al.,

Atmos. Chem. Phys. Discuss., doi:10.5194/acp-2016-874, 2016
Manuscript under review for journal Atmos. Chem. Phys.
Published: 8 November 2016

2009). Measurements of individual alkyl nitrates are more sparse. Early estimates for the total alkyl nitrate burden at rural locations influenced by urban emissions up to a few hundred pptv were derived by summing the mixing ratio of individually measured alkyl nitrates (C1 up to C8) by gas chromatography technics (Flocke et al., 1991; Flocke et al., 1998; Russo et al., 2010; Worton et al., 2010). Recent developments in chemical ionisation mass spectrometry have enabled measurement of more complex, multifunctionnal nitrates of biogenic origin and revealed the occassional presence of ppbv levels of the sum of measured alkyl nitrates (Beaver et al., 2012). Our measurements of ΣPNs and ΣANs can be more directly compared to those of the University of Califiornia at Berkeley, who have developed and applied the technique of TD-LIF over the last 15 years (Day et al., 2002; Wooldridge et al., 2010; Perring et al., 2013). The mixing ratios of ΣPNs and ΣANs at the Taunus Observatory are comparable to summertime measurements of ΣPNs and ΣANs (0 – 2 ppbv and 0 – 1 ppbv, respectively) at forested sites in California (Day et al., 2003; Murphy et al., 2006; Day et al., 2008).

4.2 Sequestering of NOx as organic nitrates

In this section, we examine how much NO*x* is sequestered as organic nitrates at this site. As HNO_3 was not measured during either campaign, we cannot examine the relative efficiency of NO*x* conversion to organic nitrates compared to inorganic HNO_3, though we expect the former to dominate in air masses in the continental boundary layer that have significant anthropogenic or biogenic emissions of hydrocarbons (Day et al., 2008).

Figure 3 shows the fraction, *f*(NO*x*), of NO*x* sequestrered as organic nitrates (*f*(NO*x*) = ([ΣPNs] + [ΣANs]) / ([ΣPNs] + [ΣANs] + [NO*x*])), plotted versus [NO*x*] and color coded for temperature. It clearly shows that *f*(NO*x*) is higher at low NO*x*, and could be as high as 0.75 in air masses containing less than 2 ppbv of NO*x*. The lowest values of *f*(NO*x*) measured (< 0.08) were associated with levels of NO*x* in excess of 10 ppbv. At this location, high values of NO_2 are associated with freshly emitted anthopogenic pollution originating from the nearby urban centres. The high values of *f*(NO*x*) during periods of low NO*x* is the result of efficient conversion of NO*x* to longer lived organic nitrates in photochemically aged air masses at this site and also suggests that organic nitrate formation is not limited by NO*x*. For a given level of NO*x*, *f*(NO*x*) is larger when temperatures are higher, reflecting stronger biogenic emissions, and more intense photochemical activity and thus conversion rates of NO*x* to organic nitrates (Olszyna et al., 1994; Day et al., 2008). Low temperatures also increase the rate of transfer of soluble organic nitrates to the aerosol phase, which acts on *f*(NO*x*) in the same direction.

4.3 Diel profiles: Photochemical and meteorological influences

Figure 4 shows the mean diel profiles of $J(O^1D)$, $[O_3]$, temperature, humidity, $[NO_2]$, [ΣPNs] and [ΣANs] for both the PARADE (red lines) and NOTOMO (black lines) campaigns. A number of factors including highly variable (temporal and spatial) local emmisions, irradiance, wind-direction and the complex topography at the site all impose their influence on the diel profiles measured for the organic nitrates.

Atmos. Chem. Phys. Discuss., doi:10.5194/acp-2016-874, 2016
Manuscript under review for journal Atmos. Chem. Phys.
Published: 8 November 2016

Atmospheric Chemistry and Physics Discussions

The mean, daily maxima in global radiation, temperature and O_3 mixing ratio were higher during NOTOMO, indicating on average warmer, sunnier and drier conditions in 2015. Lower average levels of NO_2 were measured during NOTOMO. The mean PARADE NO_2 profile shows two maxima during the day (at ~ 10:00 UTC and ~ 19:00 UTC) which correspond approximately to local rush-hour traffic increases during the working week. These NO_2 maxima are less clearly defined but still apparent in the averaged diel profiles in NOTOMO. A close inspection of the NOTOMO data revealed that the days can be divided into two types, those which display the rush-hour peaks in NO_2 (type 1, altogether seven in a total of thirty days) and those which do not (type 2) As illustrated in Fig. 5, type 1 days were associated with higher temperaures and levels of O_3 and local wind direction that has a large, daytime component from the South, whereas type 2 days were cooler, had less O_3 and the local wind had a dominant westerly component. Air masses arriving from the southerly sectors are influenced by rush-hour traffic from the nearby urban centres, whereas those arriving from the west are cleaner, with an Atlantic influence and more distant emissions of NO*x*. Up-slope winds, resulting from enhanced rates of heating of the mountainside during the warmer periods can also play a role in enhancing rates of transport of NO*x* and photochemically produced trace gases to the site compared to the cooler, cloudier days under the influence of westerly winds. During the PARADE campaign, no clear differentiation in meteorological/photo-chemical situation was possible and the diel profiles represent the entire campaign. The mean ΣPNs profiles during both campaigns (Fig. 4) indicate a growth in mixing ratio starting at about sunrise with a broad daily maxima between ≈ 12:00 and 14:00 for NOTOMO. The mean daily maximum for NOTOMO was about 1.2 ppbv, a factor of two or more than for PARADE. In contrast, during PARADE the mean daily maximum of ΣANs (≈ 0.6 ppbv) was about a factor of three larger than during NOTOMO. The ratio of the mean daily maximum of ANs to PNs, ($[ANs]_{max}$ / $[PNs]_{max}$) was thus very different for the two campaigns, with values of close to one for PARADE and ≈ 0.2 for NOTOMO.

A number of factors influence the relative concentrations of PNs and ANs. In general, higher temperatures are the result of higher levels of insolation and are thus usually related to higher O_3 concentrations and rates of photochemical processing of VOCs. This should lead to higher concentrations of both PNs and ANs. Higher levels of insolation will lead to higher NO to NO_2 ratios and elevated temperaures will reduce the lifetimes of PNs so higher temperature and more insolation both favour AN production over PN production. This is essentially the opposite to what we observe and we conclude that other factors, including the mechanism of organic nitrate production from oxidation of different VOC types and rates of depositional loss of the organic nitrates play a major role in contolling the relative abundance of ANs and PNs at this site (see later).

4.4 Daytime and night-time production of alkyl nitrates

During PARADE, the diel profiles of [ΣANs] show a maximum around 12:00 UTC, similar to the maximum in global radiation which drives primary OH formation, VOCs oxidation and peroxy radical production rates. However, as indicated in Sect. 1, ANs can also be formed by the reaction of NO_3 radicals with biogenically emitted VOCs, which can impact on their diel profile. Figure 6 shows median profiles of [ΣANs] obtained by filtering out periods with fog and rain at the site in which

Atmos. Chem. Phys. Discuss., doi:10.5194/acp-2016-874, 2016
Manuscript under review for journal Atmos. Chem. Phys.
Published: 8 November 2016

Atmospheric Chemistry and Physics Discussions

NO_3 would have been absent due to the rapid, heterogeneous scavenging of N_2O_5, with which the former is in thermal equililibrium. We also plot the mean profiles of NO_3 during these nights (representing 16 nights for PARADE and 13 nights for NOTOMO). The most notable changes compared to Fig. 4 are the increase in [ΣANs] during the night. Indeed, for the NOTOMO campaign, the night-time [ΣANs] represent almost 50 % of the day-time value. As described in Thieser et al. (2016) and Sobanski et al. (2016a), the potential artefact caused by thermal decomposition of either $ClNO_2$ or N_2O_5 (present during some nights in amounts up to several hundred pptv) in the hot inlets of the TD-CRDs was accounted for by the simultaneous measurement of both of these trace gases and therefore does not contribute to the night-time signal we ascribe to ANs.

We now explore potential meteorological and chemical contributions to the night-time increases in [ΣANs]. Sobanski et al. (2016b) report occassionally extended NO_3 lifetimes (> 1000 s) at this site that result from sampling from a low-lying residual layer. Compared to the lowest levels, the residual layer is likely to contain higer levels of photochemically generated trace gases (e.g. ANs) which would otherwise be lost by deposition. During PARADE and NOTOMO, the majority of nights were however characterised by NO_3 lifetimes of the order of minutes and less, which indicate that NO_3 is removed by reaction with VOCs, presumably mainly reactive terpenoids with double bonds. Those nights with long NO_3 lifetimes during PARADE were excluded for calculating the [NO_3]and [ΣANs] profiles in Fig. 6.

The reaction between NO_3 and unsaturated VOCs is known to produce alkyl nitrates with a higher yield than the day-time pathway through OH induced oxidation of VOCs and is a plausible explanation of the night-time maxima in ΣANs shown in Fig. 6. In order to assess this, we calculated the day and night-time production of alkyl nitrates during PARADE using measured VOCs (see Table 1). We took values from Atkinson and Arey (2003b) for the rate constants and the alkyl nitrate yields from Perring et al. (2013). For some VOCs, the alkyl nitrate yield is unknown and values were estimated based on the known yield of other, structurally similar compounds.

To estimate the night time-production of ANs, we consider the reaction between NO_2 and O_3 to be the only NO_3 precursor. Of the measured VOCs, isoprene, α-pinene, myrcene and limonene account for > 95% of the NO_3 reactivity and have large yields of ANs. The mean night-time mixing ratios for these four compounds are ≈ 15, 30, 15 and 20 ppt, respectively. The corresponding alkyl nitrate yields are 0.7, 0.15, 0.5 and 0.67, respectively, which allows us to derive a value of 0.47 for the effective alkyl nitrate yield for this VOC mixture. In the absence of laboratory investigations, the alkyl nitrate yield from NO_3 + myrcene is estimated as 50 %. Assuming that each NO_3 generated reacts rapidly with a BVOC, (this implies no significant, indirect loss of NO_3 via the heterogeneous loss of N_2O_5) and taking typical night-time [NO_2] and [O_3] mixing ratios of 2 and 40 ppbv as observed during PARADE, we calculate the production rate of ANs (Eqn. 2) to be $P(\Sigma ANs)_{night} \approx$ 70 pptv hr^{-1} which is consistent with the increase in ANs observed in the two hours following sunset during either the PARADE or NOTOMO campaigns.

$$P(\Sigma ANs)_{night} = 0.47 k_{(NO_2+O_3)}[NO_2][O_3] \quad (2)$$

Atmos. Chem. Phys. Discuss., doi:10.5194/acp-2016-874, 2016
Manuscript under review for journal Atmos. Chem. Phys.
Published: 8 November 2016

Atmospheric Chemistry and Physics Discussions

To compare the estimated night-time production with the maximum day-time production, it is necessary to know the OH concentration. During the PARADE campaign, OH was measured on only a few days that did not cover those used to derive our diel profiles. Following Bonn et al. (2014), who performed a detailed analysis of OH measurements and their correlation with $J(O^1D)$ during PARADE, we calculate $[OH] = 1.8 \times 10^{11} \times J(O^1D) \approx 3 \times 10^6$ molecule cm^{-3} for the mean [OH] between 11:00 and 13:00 UTC. For an approximate estimate of day-time ANs prodution, we take the campaign mean mixing ratios of each VOC between 11:00 and 13:00 UTC as listed in Table 1. Based on the rate coefficients and mean concentrations of the VOCs, we calculate that ≈ 54 % of production of ANs is due to terpenes, 34 % to alkenes and 7 % to alkanes.

$$P_{\Sigma ANs} = \Sigma_i \alpha_i k_{OH+RH_i}[OH][RH_i] \quad (3)$$

Using equation (3) we thus obtain a total ANs production rate of $P(\mathrm{ANS})_{\mathrm{day}} \approx 68$ pptv hr^{-1} which is very similar to the estimated night-time production. The relative rates of day- and night-time generation of ANs depends on the relative levels of OH and NO_3 (a factor ≈ 200 in favour of NO_3), the yields of ANs (generally larger for NO_3) and the rate constant for reaction with VOCs. The large night-time production rate from NO_3 degradation of VOCs in this forested enviromnent is largely a result of the selective reactivity of NO_3 towards terpenes, which have large AN yields.

Although we calculate similar production rates of ANs during the night when NO_3 is present, the daytime maximum in the ANs mixing ratio is significantly larger in both campaigns. This may be explained if the lifetime of ΣANs with respect to chemical or depositional loss is longer during the day than during the night, a consequence of enhanced deposition in a stably stratified, shallow nocturnal boundary layer and the different chemical composition and volatility of the ANs generated. The addition of NO_3 to the double bonds of terpenoids results in the generation of multifunctional, branched alkyl nitrates, with low volatility and a high propensity for condensation on aerosol. The reaction of NO_3 with e.g. limonene results in a substantial yield of organic nitrates and a mass based, secondary organic aerosol yield of ≈ 30 % (Fry et al., 2011; Fry et al., 2014). As ≈ 50 % of OH reactivity is with non-terpenoid VOCs at this site (see above), a higher fraction of mono-functionnal, linear chained alkyl nitrates are formed, which have larger vapour pressures and are less likely to condense onto particles. The lower lifetime of night-time generated ΣANs at this and other forested sites is thus likely to be the result of increased rate of aerosol scavanging of the low volatilitly ANs compared to those generated in the day, which will also be enhanced by the lower temperatures and higher relative humidities encountered at night-time. This result is consistent with ideas that the NO_3 oxidation of biogenic VOCs can lead to appreciable organo-nitrate content in atmospheric particulate matter (Fry et al., 2011; Fry et al., 2014).

Atmos. Chem. Phys. Discuss., doi:10.5194/acp-2016-874, 2016
Manuscript under review for journal Atmos. Chem. Phys.
Published: 8 November 2016

Atmospheric Chemistry and Physics Discussions

4.5 ANs yield from OH initiated VOC oxidation.

A positive correlation between organic nitrates and O_3 has been observed (Kourtidis et al., 1993; Williams et al., 1997; Roberts et al., 1998; Schrimpf et al., 1998; Day et al., 2003) and is due to the common production pathways of these trace gases. In rural and semi-rural locations, the build up of O_3 during the day is related to the NO*x* catalysed photo-oxidation of VOCs, including the reaction of organic peroxy radicals with NO*x*. These processes also dominate the daytime production of organic nitrates. As discussed in Sect. 1, alkyl nitrates are produced via a minor branch of the reaction between NO and organic peroxy radical, while the majority of reactive collisions result in the formation of NO_2 and (via its photolysis) the formation of O_3 (reaction R4 to R5). Laboratory experiments have shown that the branching ratio to ANs is strongly dependent on the identity of the peroxy radical and also varies with temperature and pressure (Perring et al., 2013). As we measure total alkyl nitrates, the effective branching ratio is determined by the particular VOC mixture encountered. Following the methodology developed by the Berkeley group (Day et al., 2003; Rosen et al., 2004) the production rates of O_3 (P_{O3}) is given by eqn. (4).

$$P_{O3} = \Sigma_i \gamma_i (1 - \alpha_i) k_{(OH+RH_i}[OH][RH_i] \quad \text{Eq. (4)}$$

where α is the branching ratio to nitrate formation in the reaction between the organic peroxy radical and NO, and γ is the number of O_3 produced per VOC oxidized, which can be between one and three but is equal to two for many atmospherically relevant VOCs, given sufficient NO (see Table 1) (Rosen et al., 2004). This can be combined with eqn. (3) to give:

$$\frac{\Delta O_3}{\Delta \Sigma ANs} = \frac{\int (P_{O3} - D_{O3} + E_{O3}) dt}{\int (P_{\Sigma ANs} - D_{\Sigma ANs} + E_{\Sigma ANs}) dt} \quad \text{Eq. (5)}$$

$$\frac{\Delta O_3}{\Delta \Sigma ANs} = \frac{2(1-\alpha)}{\alpha} \approx \frac{2}{\alpha} \quad \text{Eq. (6)}$$

In which D and E represent terms for deposition and entrainment, respectively. The ratio of O_3 to ΣANs after the OH oxidation of a VOC mixture has proceeded for a certain time, *dt*, is given by Eq. (5). At sufficiently high levels of OH, VOCs and NO, the photochemical production terms can be assumed to be larger than the loss terms and Eq. (5) simplifies to Eq. (6). In principal, a plot of [O_3] versus [ΣANs] should then yield a straight line, with a slope that is proportional to an average value of the branching ratio to ANs. The values of α we calculate using the measurement of ΣANs and O_3 is designated $\alpha_{av}^{\Sigma ANs}$. Alternatively, an average value of α can be calculated from measurement of the VOCs that react with OH, their rate constant and the individual yield of alkyl nitrate from each reaction and the O_3 yield, which we then designate α_{av}^{VOCi}.

For both the PARADE and NOTOMO campaigns, we analysed the mixing ratios of ANs and O_3 between 11:00 and 13:00 UTC (around the peak in OH levels) to calculate $\alpha_{av}^{\Sigma ANs}$. The results, displayed in Fig. 7, indicate a value of $\alpha_{av}^{\Sigma ANs}$ $(PARADE) = 7.2 \pm 0.5$ % ($R^2 = 0.49$). The intercept, 28.6 ± 1.2 ppbv, is indicative of background levels of O_3. In the

Atmos. Chem. Phys. Discuss., doi:10.5194/acp-2016-874, 2016
Manuscript under review for journal Atmos. Chem. Phys.
Published: 8 November 2016

Atmospheric Chemistry and Physics Discussions

NOTOMO dataset, the yield of ANs is low and the data very scattered with a poor correlation coefficient, hence no fit was carried out and we simply plot (black lines) two lines which encompass the whole dataset with corresponding values of α equal to 0.5 % and 1.7 % which is significantly lower than the derived α for PARADE. For NOTOMO, in which low mixing ratios of ANs were encountered, the vertical grouping of the data apparent in Fig. 7 (i.e. low resolution in concentration) is a result of the corrective procedure for extracting mixing ratios from raw data obtained in the hot and cold inlets, which involves iterative numerical simulation which converges when 1% agreement between observation and simulation is achieved (Sobanski et al., 2016a).

For the PARADE campaign, during which VOCs were measured, we derive a value of $\alpha_{\mathrm{av}}^{\mathrm{VOCi}}(PARADE) = 5.9$ % for the same period around noon (UTC) which is consistent with that derived from measured ΣANs and [O_3]. Irrespective of method used to derive the branching ratio to AN formation, the high values obtained reflect the fact that a significant fraction of OH reactivity is due to biogenic VOCs (especially terpenoids including isoprene, monoterpenes and sesquiterpenes), that have large yields of alkyl nitrates.

To some extent, the agreement may be fortuitous as both methods to derive α_{av} involve assumptions that may be only partially applicable. The value of $\alpha_{\mathrm{av}}^{\mathrm{VOCi}}$ calculated using individual VOC measurements and their respective alkyl nitrate yields is associated with a rather large uncertainty as it assumes that all VOCs with which OH reacts were actually measured during the campaign and that their alkyl nitrate yields are well known. For example, the products of isoprene oxidation, methyl-vinyl-ketone and methacrolein have high reported α values (Paulot et al., 2009) and high rate constants for reaction with OH which, if taken into account would increase the overall calculated α value. Regarding the individual nitrate yields, some values used to calculate the average (see Table 1) are not precisely determined in the literature while others are estimated. For example, the reported yields of alkyl nitrates in the reaction of OH with isoprene in the presence of NO*x* ranges from 4 to 15% (Perring et al., 2013). This analysis will also be biased if e.g. local emissions of biogenics are larger than those averaged over the time period over which O_3 and ANs were formed (i.e. when plumes containing pollution from urban areas are transported to the site).

Likewise, neglecting terms for entrainment and deposition of ANs and O_3 will introduce a variable bias into calculations of $\alpha_{av}^{\Sigma\mathrm{ANs}}$. In the absence of information regarding the deposition rate of a mixture of multi-functional nitrates or O_3 to the topographically complex terrain at the Taunus Observatory a more detailed analysis is however not warranted. The analysis does however make comparison with similar analyses for ΣANs measurements possible, and our derived values of $\alpha_{av}^{\Sigma\mathrm{ANs}}$ are consistent with those summarised by Perring et al (Perring et al., 2013) who list values obtained both by observation of ANs (7.1 % > $\alpha_{av}^{\Sigma\mathrm{ANs}}$ > 0.8 %) and calculated from VOC measurements (10.6 % > $\alpha_{av}^{\mathrm{VOCi}}$ > 0.1 %) in various rural and urban locations.

The difference in $\alpha_{av}^{\Sigma\mathrm{ANs}}$ between PARADE (7.2 ± 0.5 %) and NOTOMO (< 2 %) is significant. The cause for this difference may be related to a breakdown of the assumption that depositional losses and/or entrainment of ANs and O_3 are negligible. Dry deposition is often regarded as a major sink of alkyl nitrates especially for those derived from biogenic VOCs, and

Atmos. Chem. Phys. Discuss., doi:10.5194/acp-2016-874, 2016
Manuscript under review for journal Atmos. Chem. Phys.
Published: 8 November 2016

Atmospheric Chemistry and Physics Discussions

enhanced rates of deposition loss of ANs during NOTOMO would help explain the divergence between the results obtained. The relative humidity, an important factor influencing the deposition velocity for soluble species like isoprene derived alkyl nitrates, was very similar during both campaigns with a median humidity at noon of 60% for PARADE and 57% for NOTOMO (see Fig. 4) and therefore is unlikely to have caused different deposition rates. Likewise, rates of radiative heating for the photochemically active days during both campaigns were similar, so that boundary layer evolution is also expected to be similar. A more likely explanation for the different values of α_{av} obtained is that the VOC mixture at the mountain top was different between the two years. No VOCS were measured during NOTOMO, but the recurrent damp and foggy conditions are likely to have significantly decreased emissions of BVOCs in 2015, resulting in lower rates of alkyl nitrate formation.

4. Conclusions

By measuring total organic nitrates, NO, NO_2 and NO_3 we have shown that a significant fraction (up to 75 %) of NO*x* is sequestered as gas-phase organic nitrates at this forested site with urban influence. During the 2011 PARADE campaign, ΣANs and ΣPNs were measured in similar concentrations, whereas in NOTOMO (2015) formation of ΣANs was weaker, presumably due to weaker biogenic emissions associated with lower temperatures. Based on an estimate of the OH concentration and the NO_3 production term we show that both night-time (NO_3 initiated) and daytime (OH initiated) chemistry contributes to the formation of ANs, which is reflected in their diel profile. Despite the similar production rate, daytime ANs are more abundant, possibly reflecting their lower rates of loss by deposition, a result of differing night-time versus daytime boundary layer dynamics and chemical properties of the ANs formed. The effective branching ratio to ANs formation from the OH initiated oxidation of VOCs, estimated by comparing ANs and O_3 concentrations and also from VOC analysis, is ~ 5-7 %.

Acknowledgements

We thank Heinz Bingemer for logistical support and use of the facilities at the Taunus Observatory during the NOTOMO and PARADE campaigns. We thank Horst Fischer for making the PARADE NO dataset available and the HLUG for provision of meteorological data as well as O_3 measurements. We thank DuPont for provision of a sample of the FEP TE 9568 suspension used to coat the cavity walls. This work was carried out in part fulfilment of the PhD of Nicolas Sobanski at the Johannes Gutenberg University in Mainz, Germany.

Atmos. Chem. Phys. Discuss., doi:10.5194/acp-2016-874, 2016
Manuscript under review for journal Atmos. Chem. Phys.
Published: 8 November 2016

Atmospheric Chemistry and Physics Discussions

References

Atkinson, R.: Atmospheric chemistry of VOCs and NOx, Atmos. Env., 34, 2063-2101, 2000.

Atkinson, R., and Arey, J.: Gas-phase tropospheric chemistry of biogenic volatile organic compounds: a review, Atmos. Env., 37, S197-S219, 2003a.

Atkinson, R., and Arey, J.: Atmospheric degradation of volatile organic compounds, Chem. Rev., 103, 4605-4638, doi:10.1021/cr0206420, 2003b.

Atlas, E.: Evidence for > C_3 alkyl nitrates in rural and remote atmosphere, Nature, 331, 426-428, 1988.

Ayres, B. R., Allen, H. M., Draper, D. C., Brown, S. S., Wild, R. J., Jimenez, J. L., Day, D. A., Campuzano-Jost, P., Hu, W., de Gouw, J., Koss, A., Cohen, R. C., Duffey, K. C., Romer, P., Baumann, K., Edgerton, E., Takahama, S., Thornton, J. A., Lee, B. H., Lopez-Hilfiker, F. D., Mohr, C., Wennberg, P. O., Nguyen, T. B., Teng, A., Goldstein, A. H., Olson, K., and Fry, J. L.: Organic nitrate aerosol formation via NO_3 + biogenic volatile organic compounds in the southeastern United States, Atmos. Chem. Phys., 15, 13377-13392, doi:10.5194/acp-15-13377-2015, 2015.

Beaver, M. R., St Clair, J. M., Paulot, F., Spencer, K. M., Crounse, J. D., LaFranchi, B. W., Min, K. E., Pusede, S. E., Wooldridge, P. J., Schade, G. W., Park, C., Cohen, R. C., and Wennberg, P. O.: Importance of biogenic precursors to the budget of organic nitrates: observations of multifunctional organic nitrates by CIMS and TD-LIF during BEARPEX 2009, Atmos. Chem. Phys., 12, 5773-5785, doi:doi:10.5194/acp-12-5773-2012, 2012.

Blanchard, P., Shepson, P. B., Schiff, H. I., and Drummond, J. W.: Development of a gas chromatograph for trace gas-chromatograph for trace-level measurement of peroxyacetyl nitrate using chemical amplification, Anal. Chem., 65, 2472-2477, doi:10.1021/ac00066a012, 1993.

Bonn, B., Bourtsoukidis, E., Sun, T. S., Bingemer, H., Rondo, L., Javed, U., Li, J., Axinte, R., Li, X., Brauers, T., Sonderfeld, H., Koppmann, R., Sogachev, A., Jacobi, S., and Spracklen, D. V.: The link between atmospheric radicals and newly formed particles at a spruce forest site in Germany, Atmos. Chem. Phys., 14, 10823-10843, doi:10.5194/acp-14-10823-2014, 2014.

Browne, E. C., Perring, A. E., Wooldridge, P. J., Apel, E., Hall, S. R., Huey, L. G., Mao, J., Spencer, K. M., St Clair, J. M., Weinheimer, A. J., Wisthaler, A., and Cohen, R. C.: Global and regional effects of the photochemistry of $CH_3O_2NO_2$: evidence from ARCTAS, Atmos. Chem. Phys., 11, 4209-4219, doi:doi:10.5194/acp-11-4209-2011, 2011.

Browne, E. C., Min, K. E., Wooldridge, P. J., Apel, E., Blake, D. R., Brune, W. H., Cantrell, C. A., Cubison, M. J., Diskin, G. S., Jimenez, J. L., Weinheimer, A. J., Wennberg, P. O., Wisthaler, A., and Cohen, R. C.: Observations of total $RONO_2$ over the boreal forest: NO*x* sinks and HNO_3 sources, Atmos. Chem. Phys., 13, 4543-4562, doi:10.5194/acp-13-4543-2013, 2013.

Buhr, M. P., Parrish, D. D., Norton, R. B., Fehsenfeld, F. C., Sievers, R. E., and Roberts, J. M.: Contribution of Organic Nitrates to the Total Reactive Nitrogen Budget at a Rural Eastern U.S. Site, J. Geophys. Res., 95, 9809-9816, 1990.

Crowley, J. N., Schuster, G., Pouvesle, N., Parchatka, U., Fischer, H., Bonn, B., Bingemer, H., and Lelieveld, J.: Nocturnal nitrogen oxides at a rural mountain site in south-western Germany, Atmos. Chem. Phys., 10, 2795-2812, 2010.

Day, D. A., Wooldridge, P. J., Dillon, M. B., Thornton, J. A., and Cohen, R. C.: A thermal dissociation laser-induced fluorescence instrument for in situ detection of NO_2, peroxy nitrates, alkyl nitrates, and HNO_3, J. Geophys. Res. -Atmos., 107, doi:doi:10.1029/2001jd000779, 2002.

Day, D. A., Dillon, M. B., Wooldridge, P. J., Thornton, J. A., Rosen, R. S., Wood, E. C., and Cohen, R. C.: On alkyl nitrates, O_3, and the "missing NOy", J. Geophys. Res. -Atmos., 108, 4501, doi:doi:10.1029/2003jd003685, 2003.

Day, D. A., Wooldridge, P. J., and Cohen, R. C.: Observations of the effects of temperature on atmospheric HNO3, Sigma ANs, Sigma PNs, and NOx: evidence for a temperature-dependent HOx source, Atmos. Chem. Phys., 8, 1867-1879, 2008.

Fahey, D. W., Hübler, G., Parrish, D. D., Williams, E. J., Norton, R. B., Ridley, B. A., Singh, H. B., Liu, S. C., and Fehsenfeld, F. C.: Reactive Nitrogen Species in the Troposphere: Measurements of NO, NO_2, HNO_3, Particulate Nitrate, Peroxyacetyl Nitrate (PAN), O_3, and Total Reactive Odd Nitrogen (NO_y) at Niwot Ridge, Colorado, J. Geophys. Res., 91, 9781-9793, 1986.

Flocke, F., Volz-Thomas, A., and Kley, D.: Measurements of alkyl nitrates in rural and polluted air masses, Atmospheric Environment. Part A. General Topics, 25, 1951-1960, 1991.

Flocke, F., Volz-Thomas, A., Buers, H. J., Patz, W., Garthe, H. J., and Kley, D.: Long-term measurements of alkyl nitrates in southern Germany 1. General behavior and seasonal and diurnal variation, J. Geophys. Res. -Atmos., 103, 5729-5746, 1998.

Fry, J. L., Kiendler-Scharr, A., Rollins, A. W., Brauers, T., Brown, S. S., Dorn, H. P., Dube, W. P., Fuchs, H., Mensah, A., Rohrer, F., Tillmann, R., Wahner, A., Wooldridge, P. J., and Cohen, R. C.: SOA from limonene: role of NO3 in its generation and degradation, Atmos. Chem. Phys., 11, 3879-3894, doi:10.5194/acp-11-3879-2011, 2011.

Fry, J. L., Draper, D. C., Barsanti, K. C., Smith, J. N., Ortega, J., Winkle, P. M., Lawler, M. J., Brown, S. S., Edwards, P. M., Cohen, R. C., and Lee, L.: Secondary Organic Aerosol Formation and Organic Nitrate Yield from NO_3 Oxidation of Biogenic Hydrocarbons, Env. Sci. Tech., 48, 11944-11953, doi:10.1021/es502204x, 2014.

IUPAC: Task Group on Atmospheric Chemical Kinetic Data Evaluation, (Ammann, M., Cox, R.A., Crowley, J.N., Jenkin, M.E., Mellouki, A., Rossi, M. J., Troe, J. and Wallington, T. J.) http://iupac.pole-ether.fr/index.html., http://iupac.pole-ether.fr/index.html., 2016.

Kourtidis, K. A., Fabian, P., Zerefos, C., and Rappengluck, B.: Peroxyacetyl Nitrate (Pan), Peroxypropionyl Nitrate (Ppn) and Pan Ozone Ratio Measurements at 3 Sites in Germany, Tellus Series B-Chemical and Physical Meteorology, 45, 442-457, doi:DOI 10.1034/j.1600-0889.1993.t01-3-00004.x, 1993.

LaFranchi, B. W., Wolfe, G. M., Thornton, J. A., Harrold, S. A., Browne, E. C., Min, K. E., Wooldridge, P. J., Gilman, J. B., Kuster, W. C., Goldan, P. D., de Gouw, J. A., McKay, M., Goldstein, A. H., Ren, X., Mao, J., and Cohen, R. C.: Closing the peroxy acetyl nitrate budget: observations of acyl peroxy nitrates (PAN, PPN, and MPAN) during BEARPEX 2007, Atmos. Chem. Phys., 9, 7623-7641, doi:doi:10.5194/acp-9-7623-2009, 2009.

Lelieveld, J., Gromov, S., Pozzer, A., and Taraborrelli, D.: Global tropospheric hydroxyl distribution, budget and reactivity, Atmos. Chem. Phys. Discuss., 2016, 1-25, doi:10.5194/acp-2016-160, 2016.

Li, J., Reiffs, A., Parchatka, U., and Fischer, H.: In situ measurements of atmospheric CO and its correlation with NOx and O_3 at a rural mountain site, Metrol. Meas. Sys. , XXII, 25-38, 2015.

Murphy, J. G., Thornton, J. A., Wooldridge, P. J., Day, D. A., Rosen, R. S., Cantrell, C., Shetter, R. E., Lefer, B., and Cohen, R. C.: Measurements of the sum of HO_2NO_2 and $CH_3O_2NO_2$ in the remote troposphere, Atmos. Chem. Phys., 4, 377-384, 2004.

Murphy, J. G., Day, A., Cleary, P. A., Wooldridge, P. J., and Cohen, R. C.: Observations of the diurnal and seasonal trends in nitrogen oxides in the western Sierra Nevada, Atmos. Chem. Phys., 6, 5321-5338, 2006.

Nault, B. A., Garland, C., Pusede, S. E., Wooldridge, P. J., Ullmann, K., Hall, S. R., and Cohen, R. C.: Measurements of $CH_3O_2NO_2$ in the upper troposphere, Atmos. Meas. Tech., 8, 987-997, doi:doi:10.5194/amt-8-987-2015, 2015.

Ng, N. L., Brown, S. S., Archibald, A. T., Atlas, E., Cohen, R. C., Crowley, J. N., Day, D. A., Donahue, N. M., Fry, J. L., Fuchs, H., Griffin, R. J., Guzman, M. I., Hermann, H., Hodzic, A., Iinuma, Y., Jimenez, J. L., Kiendler-Scharr, A., Lee, B. H., Luecken, D. J., Mao, J., McLaren, R., Mutzel, A., Osthoff, H. D., Ouyang, B., Picquet-Varrault, B., Platt, U., Pye, H. O. T., Rudich, Y., Schwantes, R. H., Shiraiwa, M., Stutz, J., Thornton, J. A., Tilgner, A., Williams, B. J., and Zaveri, R. A.: Nitrate radicals and biogenic volatile organic compounds: oxidation, mechanisms and organic aerosol, Atmos. Chem. Phys. Discuss., 2016, 1-111, doi:10.5194/acp-2016-734, 2016.

Olszyna, K. J., Bailey, E. M., Simonaitis, R., and Meagher, J. F.: O_3 and NOy relationships at a rural Site, J. Geophys. Res. -Atmos., 99, 14557-14563, doi:Doi 10.1029/94jd00739, 1994.

Paulot, F., Crounse, J. D., Kjaergaard, H. G., Kroll, J. H., Seinfeld, J. H., and Wennberg, P. O.: Isoprene photooxidation: new insights into the production of acids and organic nitrates, Atmos. Chem. Phys., 9, 1479-1501, 2009.

Perring, A. E., Pusede, S. E., and Cohen, R. C.: An observational perspective on the atmospheric impacts of alkyl and multifunctional nitrates on ozone and secondary organic aerosol, Chem. Rev., 113, 5848-5870, doi:doi:10.1021/cr300520x, 2013.

Phillips, G. J., Tang, M. J., Thieser, J., Brickwedde, B., Schuster, G., Bohn, B., Lelieveld, J., and Crowley, J. N.: Significant concentrations of nitryl chloride observed in rural continental Europe associated with the influence of sea salt chloride and anthropogenic emissions, Geophys. Res. Lett., 39, L10811, doi:10.1029/2012GL051912, 2012.

Ridley, B. A., Shetter, J. D., Walega, J. G., Madronich, S., Elsworth, C. M., Grahek, F. E., Fehsenfeld, F. C., Norton, R. B., Parrish, D. D., Hübler, G., Buhr, M., Williams, E. J., Allwine, E. J., and Westberg, H. H.: The Behavior of Some Organic Nitrates at Boulder and Niwot Ridge, Colorado, J. Geophys. Res., 95, 13949-13961, 1990.

Roberts, J. M., Fajer, R. W., and Springston, S. R.: Capillary gas-chromatographic separation of alkyl nitrates and peroxycarboxylic nitric anhydrides Anal. Chem., 61, 771-772, doi:10.1021/ac00182a026, 1989.

Roberts, J. M.: The atmospheric chemistry of organic nitrates, Atmospheric Environment. Part A. General Topics, 24, 243-287, 1990.

Roberts, J. M., Bertman, S. B., Parrish, D. D., Fehsenfeld, F. C., Jobson, B. T., and Niki, H.: Measurement of alkyl nitrates at Chebogue Point, Nova Scotia during the 1993 North Atlantic Regional Experiment (NARE) intensive, J. Geophys. Res. -Atmos., 103, 13569-13580, 1998.

Roberts, J. M., Marchewka, M., Bertman, S. B., Sommariva, R., Warneke, C., de Gouw, J., Kuster, W., Goldan, P., Williams, E., Lerner, B. M., Murphy, P., and Fehsenfeld, F. C.: Measurements of PANs during the New England air quality study 2002, J. Geophys. Res. -Atmos., 112, doi:Artn D20306, 10.1029/2007jd008667, 2007.

Rollins, A. W., Pusede, S., Wooldridge, P., Min, K. E., Gentner, D. R., Goldstein, A. H., Liu, S., Day, D. A., Russell, L. M., Rubitschun, C. L., Surratt, J. D., and Cohen, R. C.: Gas/particle partitioning of total alkyl nitrates observed with TD-LIF in Bakersfield, J. Geophys. Res. -Atmos., 118, 6651-6662, doi:10.1002/jgrd.50522, 2013.

Rosen, R. S., Wood, E. C., Wooldridge, P. J., Thornton, J. A., Day, D. A., Kuster, W., Williams, E. J., Jobson, B. T., and Cohen, R. C.: Observations of total alkyl nitrates during Texas Air Quality Study 2000: Implications for O_3 and alkyl nitrate photochemistry, J. Geophys. Res. -Atmos., 109, Art. Nr D07303, doi:doi:10.1029/2003jd004227, 2004.

Russo, R. S., Zhou, Y., Haase, K. B., Wingenter, O. W., Frinak, E. K., Mao, H., Talbot, R. W., and Sive, B. C.: Temporal variability, sources, and sinks of C_1-C_5 alkyl nitrates in coastal New England, Atmos. Chem. Phys., 10, 1865-1883, 2010.

Schrimpf, W., Linaerts, K., Muller, K. P., Koppmann, R., and Rudolph, J.: Peroxyacetyl nitrate (PAN) measurements during the POPCORN campaign, J. Atmos. Chem., 31, 139-159, doi:Doi 10.1023/A:1006004031055, 1998.

Schuster, G., Labazan, I., and Crowley, J. N.: A cavity ring down / cavity enhanced absorption device for measurement of ambient NO_3 and N_2O_5, Atmos. Meas. Tech., 2, 1-13, 2009.

Schwantes, R. H., Teng, A. P., Nguyen, T. B., Coggon, M. M., Crounse, J. D., St Clair, J. M., Zhang, X., Schilling, K. A., Seinfeld, J. H., and Wennberg, P. O.: Isoprene NO_3 Oxidation Products from the RO_2 + HO_2 Pathway, J. Phys. Chem. A, 119, 10158-10171, doi:10.1021/acs.jpca.5b06355, 2015.

Sobanski, N., Schuladen, J., Schuster, G., Lelieveld, J., and Crowley, J.: A 5-channel cavity ring-down spectrometer for the detection of NO_2, NO_3, N_2O_5, total peroxy nitrates and total alkyl nitrates, Atmos. Meas. Tech. Discuss., 2016, 1-32, doi:10.5194/amt-2016-191, 2016a.

Sobanski, N., Tang, M. J., Thieser, J., Schuster, G., Pöhler, D., Fischer, H., Song, W., Sauvage, C., Williams, J., Fachinger, J., Berkes, F., Hoor, P., Platt, U., Lelieveld, J., and Crowley, J. N.: Chemical and meteorological influences on the lifetime of NO_3 at a semi-rural mountain site during PARADE, Atmos. Chem. Phys., 16, 4867-4883, doi:10.5194/acp-16-4867-2016, 2016b.

Thieser, J., Schuster, G., Phillips, G. J., Reiffs, A., Parchatka, U., Pöhler, D., Lelieveld, J., and Crowley, J. N.: A two-channel, thermal dissociation cavity-ringdown spectrometer for the detection of ambient NO_2, RO_2NO_2 and $RONO_2$, Atmos. Meas. Tech., 9, 553-576, 2016.

Williams, J., Roberts, J. M., Fehsenfeld, F. C., Bertman, S. B., Buhr, M. P., Goldan, P. D., Hubler, G., Kuster, W. C., Ryerson, T. B., Trainer, M., and Young, V.: Regional ozone from biogenic hydrocarbons deduced from airborne measurements of PAN, PPN, and MPAN, Geophys. Res. Lett., 24, 1099-1102, 1997.

Williams, J., Roberts, J. M., Bertman, S. B., Stroud, C. A., Fehsenfeld, F. C., Baumann, K., Buhr, M. P., Knapp, K., Murphy, P. C., Nowick, M., and Williams, E. J.: A method for the airborne measurement of PAN, PPN, and MPAN, JGR, 105, 28943-28960, 2000.

Wooldridge, P. J., Perring, A. E., Bertram, T. H., Flocke, F. M., Roberts, J. M., Singh, H. B., Huey, L. G., Thornton, J. A., Wolfe, G. M., Murphy, J. G., Fry, J. L., Rollins, A. W., LaFranchi, B. W., and Cohen, R. C.: Total Peroxy Nitrates (ΣPNs) in the atmosphere: the Thermal Dissociation-Laser Induced Fluorescence (TD-LIF) technique and comparisons to speciated PAN measurements, Atmos. Meas. Tech., 3, 593-607, doi:doi:10.5194/amt-3-593-2010, 2010.

Worton, D. R., Reeves, C. E., Penkett, S. A., Sturges, W. T., Slemr, J., Oram, D. E., Bandy, B. J., Bloss, W. J., Carslaw, N., Davey, J., Emmerson, K. M., Gravestock, T. J., Hamilton, J. F., Heard, D. E., Hopkins, J. R., Hulse, A., Ingram, T., Jacob, M. J., Lee, J. D., Leigh, R. J., Lewis, A. C., Monks, P. S., and Smith, S. C.: Alkyl nitrate photochemistry during the tropospheric organic chemistry experiment, Atmos. Env., 44, 773-785, 2010.

Atmos. Chem. Phys. Discuss., doi:10.5194/acp-2016-874, 2016
Manuscript under review for journal Atmos. Chem. Phys.
Published: 8 November 2016

Atmospheric Chemistry and Physics Discussions

Table 1. VOCs measured during the PARADE campaign by GC-MS/FID

VOC	Mean noon time mixing ratio (ppbv)	$k_{OH + VOC}$ (cm^3 $molecule^{-1}$)	α(ANs)	P(ANs) (pptv hr^{-1})	$P(O_3)$ (pptv hr^{-1})
limonene	28	1.71×10^{-10}	0.28	15	75
butadiene	240	6.6×10^{-11}	0.07	12	320
1-pentene	560	3.14×10^{-11}	0.05[b]	9.5	358
myrcene	20	2.15×10^{-10}	0.18[b]	8.5	75
α-pinene[a]	49	5.37×10^{-11}	0.18	5.3	66
i-pentane[a]	282	3.9×10^{-12}	0.35[b]	4.3	22
isoprene	85	1.01×10^{-10}	0.044	4	178
ethylbenzene	26	7.10×10^{-11}	0.1[b]	2	36
benzene	78	1.23×10^{-11}	0.1[b]	1.1	19
n-Pentane[a]	211	3.9×10^{-12}	0.105	1	23
i-Butane[a]	131	2.33×10^{-112}	0.255	0.85	7
toluene	126	6.0×10^{-12}	0.1[b]	0.83	15
m-xylene	46	1.43×10^{-11}	0.1[b]	0.73	13
p-xylene	46	1.43×10^{-11}	0.1[b]	0.73	13
n-Butane[a]	265	2.54×10^{-12}	0.077	0.6	19
hexane	56	5.61×10^{-12}	0.141	0.48	8.3
propene	105	2.63×10^{-11}	0.015	0.45	58
o-xylene	21	1.37×10^{-11}	0.0086	0.33	5.8
cis-2-Butene	15	5.6×10^{-11}	0.037[b]	0.33	17
propane	330	1.15×10^{-12}	0.036	0.15	7.9
ethane	590	2.6×10^{-13}	0.019	0.033	3.3
p-cymene	5	1.51×10^{-11}	0.03	0.025	1.5
ethene	246	8.5×10^{-12}	0.0086	0.02	45
methane	1.8×10^{6}	6.9×10^{-15}	0	0	268
HCHO	1940	8.5×10^{-12}	0	0	358
CO	1.2×10^{5}	2.4×10^{-13}	0	0	303
Sum				**68.3**	**2314.8**

The production rate of alkyl nitrates and O_3 are calculated based on an OH concentration of 3×10^6 molecule cm^{-3}. VOCs are sorted by decreasing production rate of alkyl nitrates. The number of ozone molecules produced per VOC oxidized is taken to be two unless otherwise designated. [a] 2.85 O_3 per VOC oxidised (Rosen et al., 2004). [b] the alkyl nitrate yield is estimated based on the compound structure similarity with other alkyl nitrate yield known coumpounds (Rosen et al., 2004).

Atmos. Chem. Phys. Discuss., doi:10.5194/acp-2016-874, 2016
Manuscript under review for journal Atmos. Chem. Phys.
Published: 8 November 2016

Atmospheric Chemistry and Physics Discussions

Table 2. Minimum, mean and maximum values for relative humidity, temperature, ozone, NO, NO_2 and organic nitrates during the PARADE and NOTOMO campaign.

	PARADE (2011)			NOTOMO (2015)		
Species	Minimum	Maximum	Mean	Minimum	Maximum	Mean
Relative humidity (%)	38	100	77	27	100	70
Temperature (°C)	6	27	15	6	33	17
O_3 (ppbv)	8	81	41	17	150	48
NO_2 (ppbv)	0.3	21	2.7	0.1	15	2
NO (ppbv)	< LOD	5	0.3	0[a]	3[a]	0.3[a]
ΣPNs (ppbv)	< LOD	2	0.5	< LOD	3.2	0.7
ΣANs (ppbv)	< LOD	1.2	0.3	< LOD	0.8	0.1

[a] calculated from photo-stationary state (see text for details).

Atmos. Chem. Phys. Discuss., doi:10.5194/acp-2016-874, 2016
Manuscript under review for journal Atmos. Chem. Phys.
Published: 8 November 2016

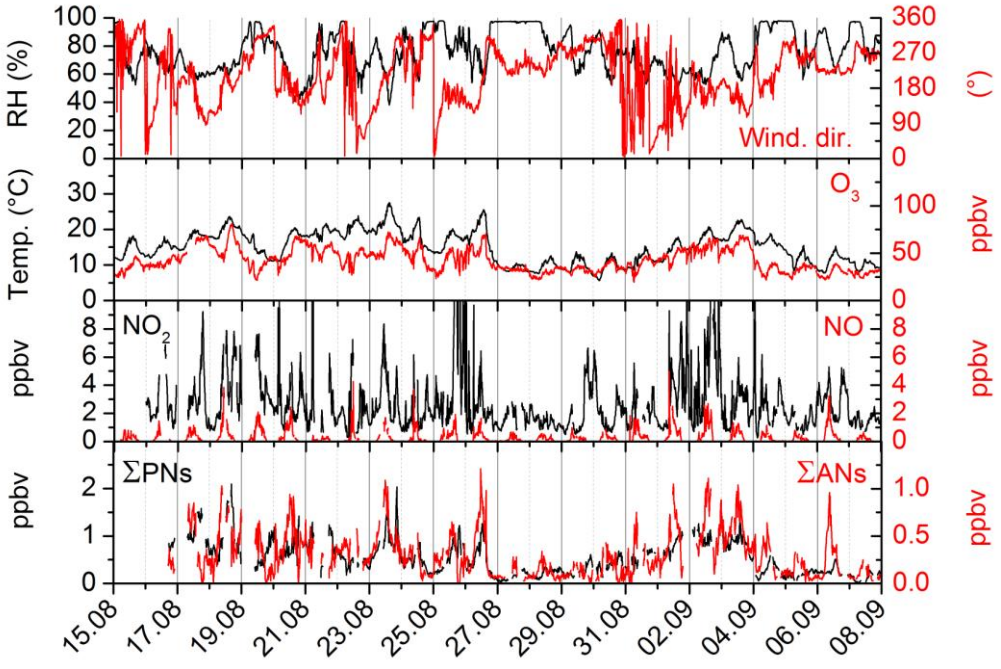

Fig. 1. PARADE 2011: Time-series of relative humidity (RH), wind direction, temperature, and the O_3, NO_2, NO, ΣPNs, and ΣANs mixing ratios.

Atmos. Chem. Phys. Discuss., doi:10.5194/acp-2016-874, 2016
Manuscript under review for journal Atmos. Chem. Phys.
Published: 8 November 2016

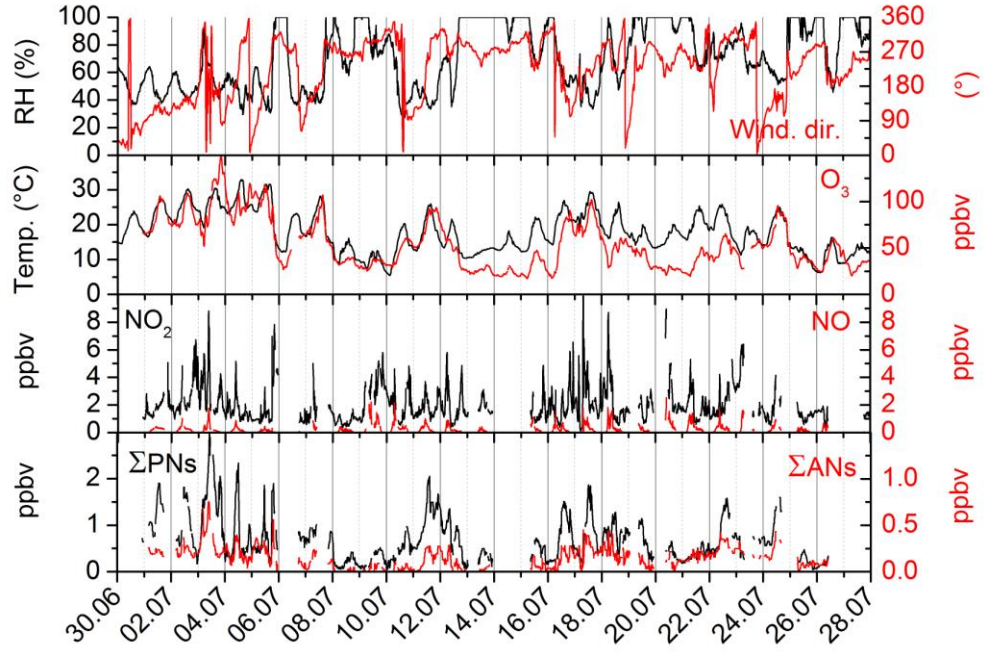

Fig. 2. NOTOMO 2015: Time-series of relative humidity (RH), wind direction, temperature, and the O_3, NO_2, NO, ΣPNs, and ΣANs mixing ratios. The NO mixing ratios were calculated assuming photo-stationary state as described in the text.

Atmos. Chem. Phys. Discuss., doi:10.5194/acp-2016-874, 2016
Manuscript under review for journal Atmos. Chem. Phys.
Published: 8 November 2016

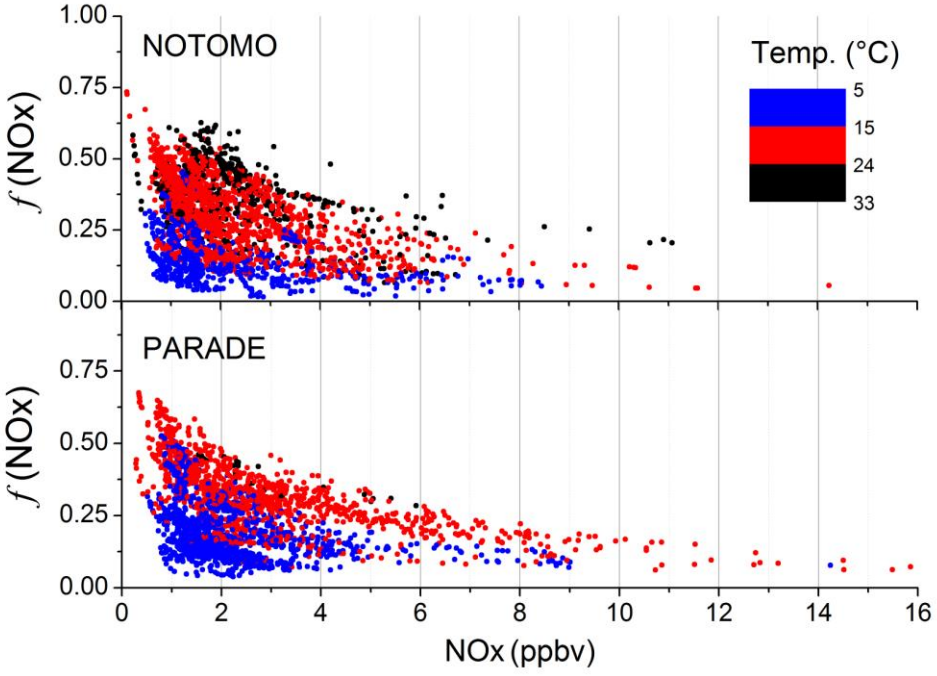

Fig. 3. The fraction of NO*x* sequestered as organic nitrates *f*(NO*x*)= [ΣPNs]+[ΣANs] /([ΣPNs]+[ΣANs]+[NO*x*]) as a function of NO*x* for the NOTOMO and PARADE campaigns, both colour coded for temperature.

Atmos. Chem. Phys. Discuss., doi:10.5194/acp-2016-874, 2016
Manuscript under review for journal Atmos. Chem. Phys.
Published: 8 November 2016

Atmospheric Chemistry and Physics Discussions

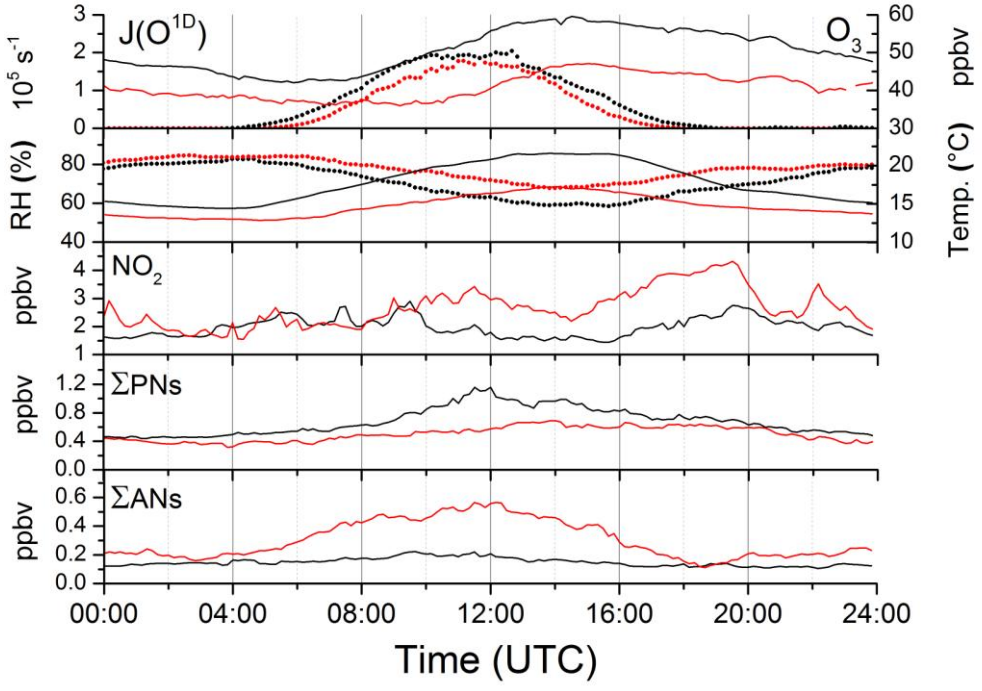

Fig. 4. Mean diel profiles during PARADE (red) and NOTOMO (black) of J(O^1D) and relative humidity (points) and [O_3], temperature, [NO_2], [ΣPNs] and [ΣANs] (lines).

Atmos. Chem. Phys. Discuss., doi:10.5194/acp-2016-874, 2016
Manuscript under review for journal Atmos. Chem. Phys.
Published: 8 November 2016

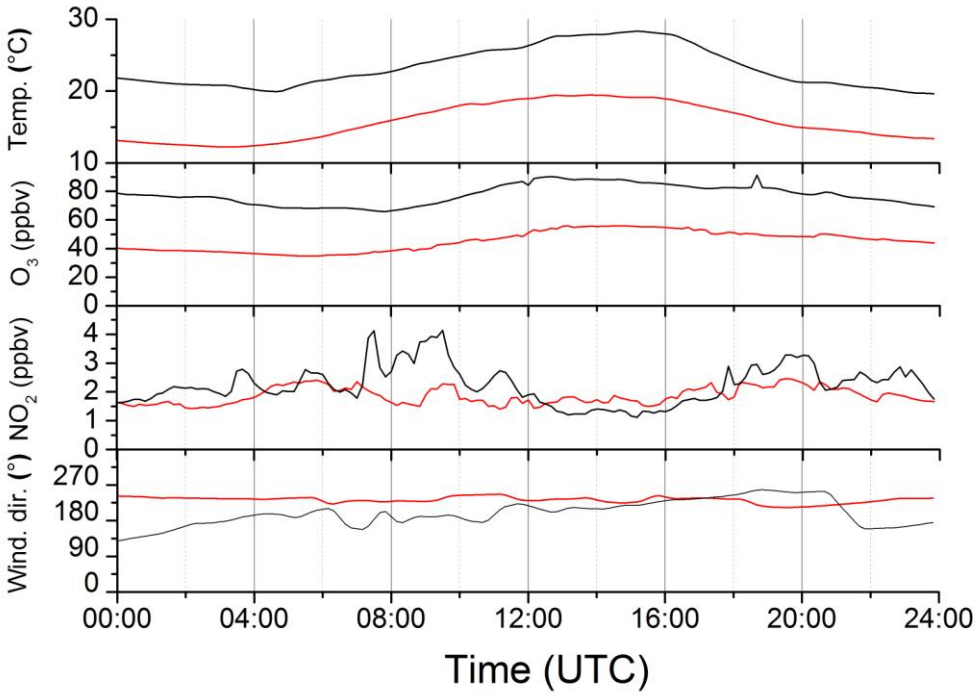

Fig. 5. Mean daily profiles of [O_3], temperature, [NO_2], and wind direction for the NOTOMO campaign separated into days with a clear influence from local rush-hour traffic (black). The rest are shown in red.

Atmos. Chem. Phys. Discuss., doi:10.5194/acp-2016-874, 2016
Manuscript under review for journal Atmos. Chem. Phys.
Published: 8 November 2016

Atmospheric Chemistry and Physics Discussions

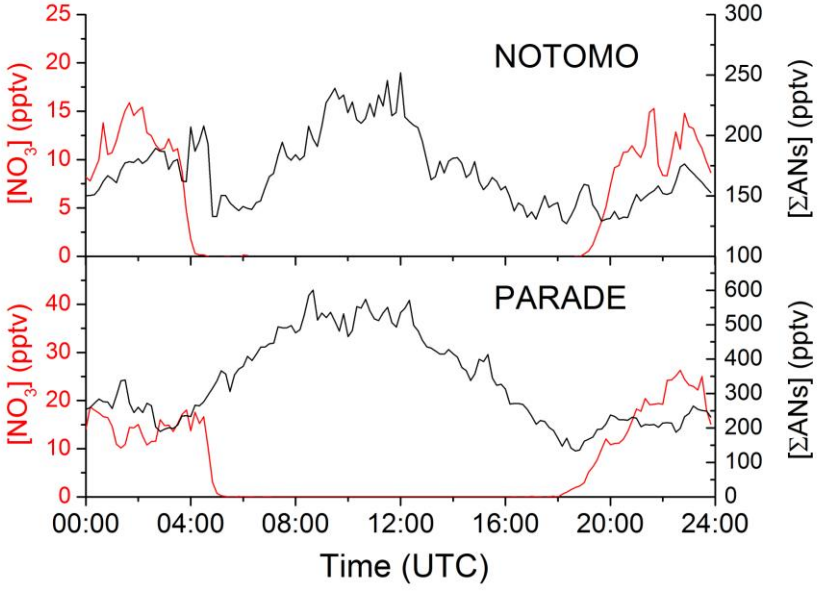

Fig. 6. Mean daily profiles of [NO_3] (red) and [ΣANs] (black) for the NOTOMO (top) and PARADE campaigns (bottom) for relative humidity < 90%.

Atmos. Chem. Phys. Discuss., doi:10.5194/acp-2016-874, 2016
Manuscript under review for journal Atmos. Chem. Phys.
Published: 8 November 2016

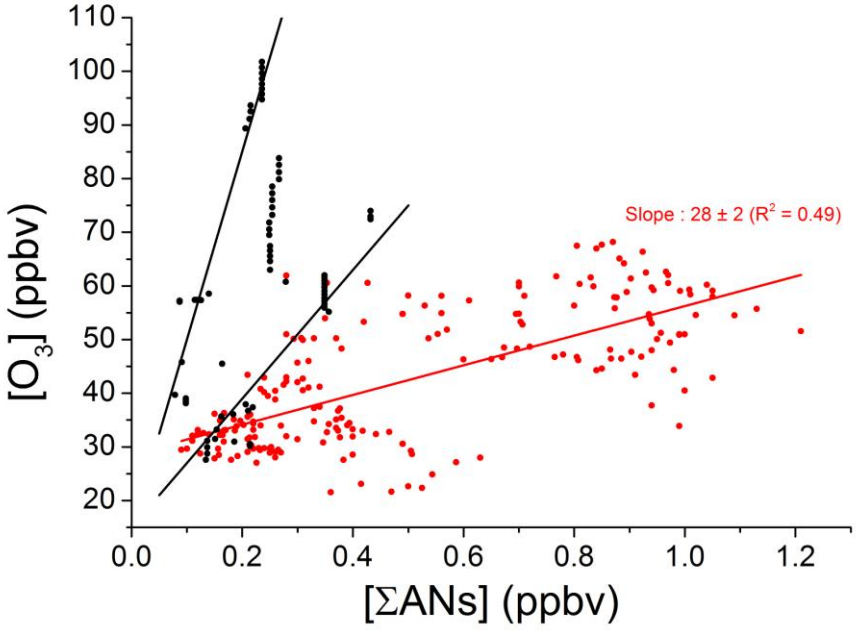

Fig. 7. [O_3] versus [ΣANs] measured between 11:00 and 13:00 UTC for the PARADE (red data points) and NOTOMO campaigns (black data points). The lines represent the best fit for the PARADE (red). For NOTOMO the black line are chosen to encompass all possible values of α assuming a background O_3 level of 15 ppbv. The apparent, poor resolution in the NOTOMO data is the result of the iterative correction procedure as described in the text.